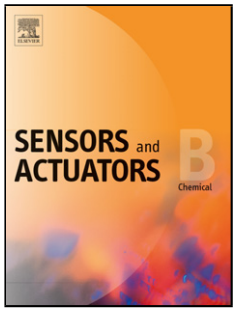

Title: Room temperature vanadium dioxide–carbon nanotube gas sensors made *via* continuous hydrothermal flow synthesis.

Authors: Gwyn P. Evans, Michael J. Powell, Ian D. Johnson, Dougal P. Howard, Dustin Bauer, Jawwad A. Darr, Ivan P. Parkin

PII: S0925-4005(17)31298-4
DOI: http://dx.doi.org/doi:10.1016/j.snb.2017.07.152
Reference: SNB 22811

To appear in: *Sensors and Actuators B*

Received date: 28-10-2016
Revised date: 24-6-2017
Accepted date: 13-7-2017

Please cite this article as: Gwyn P.Evans, Michael J.Powell, Ian D.Johnson, Dougal P.Howard, Dustin Bauer, Jawwad A.Darr, Ivan P.Parkin, Room temperature vanadium dioxide–carbon nanotube gas sensors made via continuous hydrothermal flow synthesis., Sensors and Actuators B: Chemicalhttp://dx.doi.org/10.1016/j.snb.2017.07.152

Sensors and Actuators B: Chemical

Room temperature vanadium dioxide–carbon nanotube gas sensors made *via* continuous hydrothermal flow synthesis.

Gwyn. P. Evans[a,b], Michael. J. Powell[b], Ian. D. Johnson[b], Dougal. P. Howard[b], Dustin Bauer[b], Jawwad. A. Darr[b], Ivan. P. Parkin[b,*]

[a]*Department of Security and Crime Science, University College London, 35 Tavistock Square, London, WC1H 9EZ, United Kingdom*
[b]*Department of Chemistry, University College London, Gordon Street, London, WC1H 0AJ, United Kingdom*
** Corresponding author E-mail address: i.p.parkin@ucl.ac.uk*

Abstract

Vanadium dioxide–carbon nanotube (VO_2–CNT) nanocomposite materials were produced *via* a continuous hydrothermal flow synthesis (CHFS) method. The composites were made in a single step from CHFS using dispersions of commercially available single-walled carbon nanotubes (SWCNTs) or multi-walled carbon nanotubes (MWCNTs) in a metal salt solution (aq.). The room temperature gas sensing characteristics of the VO_2-CNT nanocomposites were investigated and compared with sensors of CHFS-made VO_2 without added carbon. The VO_2-CNT nanocomposites were found to display high sensitivity to H_2O vapour, showing excellent potential as humidity sensors. Furthermore, *p*-type responses to ammonia gas were observed, with the VO_2 (no carbon) sensors showing the largest response. Overall, surface composition and microstructure were found to greatly influence sensor responses to H_2O vapour and NH_3 gas.

Keywords: Gas sensor; carbon nanotubes; vandium oxides; continous hydrothermal flow synthesis; humidity sensing; ammonia gas

1. Introduction

The synthesis of gas sensing nanomaterials at scale is important for the development of better commercial gas sensors[1,2]. Nanomaterials have shown promise for sensing of low concentrations of analyte, due to their high surface area and electronic properties that are affected by the local environment[3–5]. In some cases, the particular application and nanomaterial characteristics, permit sensor operation at room temperature, resulting in lower power consumption and increasing sensor suitability for use in portable devices[6]. The development of such materials is key to realising their application in sensors for personal health[7], environmental[8] and agricultural monitoring[9].

Metal-oxide nanomaterials have received considerable attention as gas sensitive materials[10]. Monoclinic vanadium dioxide [VO_2(M)] is a particularly interesting thermochromic material[11], with a range of polymorphs that have attracted interest for use in gas sensing[12–15]. A variety of morphologies have been obtained for vanadium oxides (VO_x), including nanofibers[16], nano-belts[17], nanorods[12,18–20] and nanowires (NWs)[13]. Gas sensors using these nanomaterials have been used for the detection of ammonia (NH_3) gas[21–23], nitrogen dioxide (NO_2)[24], ethanol (C_2H_6O)[17,25], methane (CH_4)[26] and liquefied petroleum gas (LPG)[12], at both ambient (25 ° C) and elevated operating temperatures. Strelcov *et al.* reported that by operating a VO_2 nanowire sensor close to the materials' metal-semiconductor transition temperature (≈ 68 ° C), conductance through the material became highly sensitive to the molecular composition of the environment, even enabling the detection of inert gases[13]. Depending on the structures formed and their respective oxidation states, vanadium oxides can also display sensitivity to water (H_2O) and are thus suitable for use as humidity sensors[12,14,27,28].

As well as metal oxides, carbon nanotubes have been used as the active sensing elements in chemical sensors, for the detection of a wide variety of gases and vapours at room temperature[29–31]. To increase selectivity towards a certain target molecules and reduce cross-sensitivity to other interfering species, carbons in gas sensors are often functionalised[32–36] or incorporated into a composite material[3,37–41].

Similarly, composite vanadium oxide nanostructures have previously been synthesised for gas sensing, including vanadium oxide decorated CNTs[42], VO_2(B)@ZnO heterostructured nanorods[28] and V_2O_5 doped films[43].

In this work, vanadium dioxide (B-phase)–carbon nanotube [VO_2(B)–CNT] composite materials were directly produced *via* a continuous hydrothermal flow synthesis (CHFS) method. Commercially available single-walled carbon nanotubes (SWCNTs) or multi-walled carbon nanotubes (MWCNTs), were mixed with a vanadium metal salt solution (aq.) and used as a reagent feed in a CHFS process to produce the VO_2-CNT composite materials. Controlling the nanoparticle size, shape and

microstructure is important for sensing applications, as these factors drastically affect the material's performance. Therefore, the CHFS method used herein, was beneficial as it allowed scalable synthesis of the nanomaterials (with some control over particle properties) that were then used for water and ammonia gas sensing[2,44–46].

The materials were characterised using a range of analytical methods including scanning electron microscopy (SEM), transmission electron microscopy (TEM), X-ray diffraction (XRD), X-ray photoelectron spectroscopy (XPS), current voltage (*I-V*) device characterisation, the hot-probe method and Brunauer–Emmett–Teller (BET) analysis. The sensing characteristics of the VO_2(B)-CNT gas sensors were compared with sensors containing solely VO_2(B) and with results from literature for vanadium oxide or CNT based sensors. The sensitivity to water vapour was greatly affected by the incorporation of nanotubes in the VO_2(B)-CNT composite sensing layer. This was not the case for sensing responses to low concentrations (10 to 50 ppm) of ammonia gas (NH_3), which instead, were dependent upon the surface area available for VO_2-NH_3 interactions and the material's surface composition.

To further evaluate how the nanotube-modified layer affected the VO_2(B)-CNT composite sensor responses to the analytes of interest, the materials were nitrogen doped and responses to the analytes studied were compared with un-doped samples.

Sensing mechanisms previously used to describe the responses of vanadium oxide based sensors[12] were found to be applicable in this study in conjunction with those applied to other metal oxide devices operating at room temperature.

Low powered, affordable sensors for toxic NH_3 are required for applications such as disease detection, industrial and agricultural monitoring. Likewise, simple, reliable and portable humidity sensing devices are required for novel uses in medical systems, packaging for food and consumer electronics[47,48]. Therefore, the scalable nanomaterials production methods such as CHFS are important for the development of miniaturised analytical instruments. The sensing results reported herein, are compared with those relevant in the literature with a view towards many potential humidity or NH_3 sensing applications.

2. Materials and Methods

2.1. Continuous hydrothermal flow synthesis method

Fig. 1 shows a schematic diagram of the CHFS process used herein for the production of the VO_2 nanoparticles and the VO_2-CNT composites. For the pure VO_2 sample, a vanadium(IV) precursor solution (aq.) at ambient temperature was pumped into an engineered mixer (reactor) where it was mixed with a flow of supercritical water (temperature = 450˚C, pressure = 24.1 MPa), resulting in rapid conversion of the metal salts into metal oxides *via* instantaneous hydrolysis and dehydration[46].

The lab-scale CHFS process was used, details of which, are reported elsewhere (Fig. 1)[46]. Briefly, the process is as follows; three identical diaphragm pumps (Primeroyal K, Milton Roy, Pont Saint-Pierre, France) were used to supply three pressurised feeds at 24.1 MPa. These feeds were (i) DI water at a flow rate of 80 mL min^{-1} from pump P1 (which is later heated in line), (ii) DI water or nanotube dispersions (the details of which are described below) at a flow rate of 40 mL min^{-1} (pump P2) and (iii) aqueous V-containing metal salt solution (0.05 M) flow rate of 40 mL min^{-1} (pump P3). In the CHFS process, the feeds from pumps P2 and P3 were mixed in flow using a ¼ inch stainless steel T-piece. This combined flow from P2 and P3 was then mixed with a supercritical water under turbulent conditions using a Confined Jet Mixer (CJM), which facilitates rapid formation of nanoparticles at ca. 325˚C (see Fig. 1). The design and benefits of the CJM is detailed in previous publications by some of the authors[46]. Thereafter, the particle-laden flow was then cooled to ca. 40˚C using a pipe-in-pipe heat exchanger, before passing through a back-pressure regulator (BPR), which maintained the pressure in the system. The resulting nanoparticles or nanoparticle-CNT composites were cooled and collected as a slurry in an open beaker at 25 º C after passing through a back-pressure regulator (TESCOM model 26-1762-24-194) valve. The concentrated slurry was then freeze-dried (Virtis Genesis 35XL) by slowly heating the samples from -60˚C to 25˚C over 24 h under vacuum of < 13.3 Pa. For the CHFS-made composite materials, CoMoCAT single-walled carbon nanotubes, SWCNTs (SWeNT® SG-76, CAS: 308068-56-6, purchased from Sigma-Aldrich, Dorset UK) or multi wall carbon nanotubes, MWCNTs (CAS: 698849, Sigma-Aldrich, Dorset UK) were dispersed in water (carbon concentration: 0.2 mg mL^{-1}) with aid of surfactant (sodium deoxycholate, 1 wt %) and a tip sonication probe (225 W, large volume tip for 15 minutes). This was then mixed with the aqueous vanadium (IV) salt *via* pump P-2.

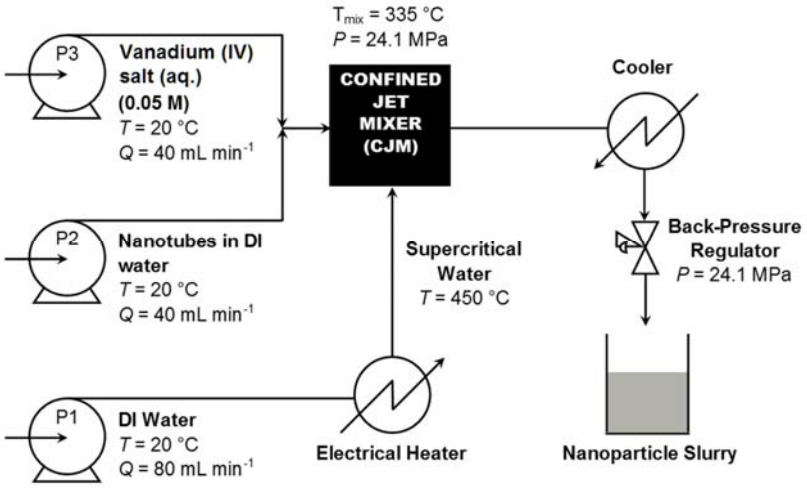

Figure. 1. Flow diagram schematic of the continuous hydrothermal synthesis (CHFS) process (adapted from Howard *et al.*[49]). DI water and premixed metal precursor solution from pumps P2 and P3 were mixed in a ¼ inch stainless steel T-piece, prior to mixing with the supercritical water flow delivered *via* pump P-1 (temperature = 450˚C, pressure = 24 MPa) in a Confined Jet Mixer (CJM). For the synthesis of VO_2-CNT composites, dispersed carbons are added in flow *via* pump P2, with the vanadium (IV) salt is delivered at ambient temperature *via* pump P3. Feeds from P2 and P3 are first mixed in-line in a tee piece (at room temperature) before the combined mixture is then mixed with the sc-water feed (delivered from P1) in the CJM (reactor). Thereafter, the products are cooled in line and recovered at atmospheric pressure as a slurry after the back-pressure regulator. For the synthesis of VO_2 with no carbons, the feed from P2 is simply DI water.

2.2. Ammonolysis treatment

An ammonolysis treatment[50] was used to N-dope the VO_2(B) control samples and the VO_2(B)-CNT samples. An alumina crucible containing the relevant powders was placed in the centre of a quartz furnace tube and anhydrous ammonia gas (BOC cylinder, 99.98 % purity) was passed through the furnace tube at a pressure of 1 mbar at room temperature and at a flow rate of 0.75 L min^{-1}. After 15 mins, the tube furnace was heated to 300˚C (ramp rate 10˚C min^{-1}) and samples were held at this temperature under the ammonia atmosphere for 1 hour. The samples were then cooled (10˚C min^{-1}) to room temperature under ammonia flow until completion; samples were then stored and handled in air.

2.3. Device Fabrication

The sensor substrates consisted of 3 × 3 mm alumina tiles with patterned gold electrodes of 175 μm separation (as shown in Fig. 2a). For each sensor type, individual substrates were placed in a grooved metal holder (heated to 40 °C *via* hot plate) and the square gold connector pads were covered using a removable mask.

The VO_2 and VO_2-CNT samples were each separately dispersed in ethanol at a concentration of 200 mg mL^{-1} and deposited on the heated sensor substrates using a calibrated Finnpipette novus electronic single-channel micro pipet (drop volume 1 μL per sensor). The deposition across the interdigitated gold electrodes was left to dry for in air for 15 min, the connector pad masks were removed and the substrates were separated into individual sensor chips.

2.4. Gas Testing Procedure

A cylindrically shaped gas-testing chamber was used with sensors equally spaced around the midpoint. The synthetic air flow rate, chamber humidity/gas mixing was controlled using digital mass flow controllers (MKS Instruments 179A general purpose mass flow controllers), being delivered at a determined concentration through a central inlet. The circular arrangement of the devices around the midpoint, along with the extraction of gas behind each individual port location, ensured that each sensor was exposed to an equal flow and concentration of gas. A potentiostat setup was used to derive the room temperature sensor conductance throughout the testing run, as described previously[2].

Dry synthetic air (BOC, composition: 21 % oxygen, 79 % nitrogen, grade: synthetic air) was passed over the sensors for 1 h (flow rate of 1.0 L min^{-1}) to obtain a baseline resistance (R_0) and achieve 0 % relative chamber humidity (confirmed using internal humidity meter). Wet air was produced by flowing a separate line of dry synthetic air though a Dreschel flask

containing 0.5 L of deionized H_2O as described previously[51]. Relative humidity (RH) is defined as the amount of water vapour in the atmosphere as a percentage of the amount of water vapour the atmosphere could hold at a specific temperature[52] (23°C in the current study). For the water vapour sensitivity testing, the relative humidity of the chamber was increased by mixing the required ratio of dry synthetic air with wet air using the mass flow controllers for 600 s (in 10 % steps from 0 to 90 % RH, ±5 % RH), followed by 1200 s of dry synthetic air to re-establish the baseline resistance of the sensors. Mixing a flow of dry air and wet air by a 50:50 ratio was defined to give 50 % RH in the chamber, as confirmed by an internal humidity meter and described previously[53]. For NH_3 testing, a cylinder of 50 ppm NH_3 (BOC cylinder, certified at 50.96 ppm in dry synthetic air, 99.98 % purity) was diluted to the desired concentration by controlled mixing with dry synthetic air *via* digital mass flow controllers (MKS Instruments 179A general-purpose mass flow controllers). Pulses of NH_3 in the 10 to 50 ppm concentration range were introduced to the testing chamber for 300 s followed by 1800 s of dry synthetic air to re-establish baseline resistance.

2.5. Characterisation

A Jeol JSM-6700F field-emission scanning electron microscope was used in secondary electron imaging mode to image the sensor surface of the VO_2(B) control, VO_2(B)-SWCNT and VO_2(B)-MWCNT samples. A 5 kV probe voltage was applied at a working distance of 3.6 mm. Samples were gold coated for imaging. Approximate particle dimensions were calculated using ImageJ image analysis software in conjunction with the statistics package in Origin Pro 9.1.

Transmission electron microscopy (TEM) was performed using a Jeol 200 kV transmission electron microscope in imaging mode. The VO_2 and VO_2-CNT samples were each separately dispersed in ethanol and drop coated onto a holey carbon coated gold TEM grid purchased from Agar Scientific for imaging.

Powder X-ray diffraction (XRD) studies were carried out on the as-synthesised CHFS powders using a Stoe (Mo) StadiP diffractometer. The instrument operated with a Mo X-ray source (Mo tube 50 kV 30 mA), monochromated (Pre-sample Ge (111) monochromator selects Kα1 only with wavelength = 0.7093 Å) and a Dectris Mython 1k silicon strip detector covering 18° in 2θ. Data was collected in transmission mode, with the sample being rotated in the X-ray beam; the diffraction patterns obtained were compared with database standards (ICSD pattern reference: 73856).

X-ray photoelectron spectroscopy (XPS) was performed using a Thermo Scientific K-alpha spectrometer with monochromated Al Kα radiation, dual beam charge compensation system and constant pass energy of 50 eV (spot size 400 μm). Survey scans were collected in the range 0–1200 eV. High-resolution peaks were used for the principal peaks of V (2p), O (1s), N (1s) and C (1s). Data was calibrated against C1s (285.0 eV).

Low-temperature nitrogen adsorption-desorption isotherms were measured at 77 K using a Quantachrome Autosorb-IQ2 machine. Specific surface area was measured using the desorption isotherm within relative pressures of 0.01 and 0.3, in accordance with the Brunauer-Emmett-Teller (BET) method.

A Keithley 4200 semiconductor characterisation system was used to obtain the current-voltage (*I* - *V*) characteristics and sensor resistances for the VO_2 and VO_2-CNT samples. The probes were contacted with the gold electrodes on each of the sensor substrates, and the instrument was set to single sweep mode from -5 V to +5 V, 0.1 V step size. The average resistances of each sensor type were calculated by averaging the $I - V$ curves for two identical sensors and taking the resistance as the ratio of V / I at 0.1 V applied potential difference.

The hot-probe method[54] was used to confirm that the VO_2 (B) control sample and the nanotube modified composites displayed *n*-type conductivity overall. The CHFS-made powders were pressed into disks of ca. 1.0 cm diameter. The potential difference across the disk was measured using a Keithley 2100/230-240 digital multimeter. A positive probe was heated to a set temperature (240 ℃) while in contact with the disks using a soldering iron tip and the induced change in potential was recorded. A positive voltage reading indicates that electrons are the majority charge carriers, thus the control and composite samples were deemed to be *n*-type semiconductors.

3. Results and Discussion

To understand the room temperature sensing results for the vanadium oxide systems studied, the composition and microstructure of the surface, the conductivity type and the components of the sensing layer that contributed towards conduction were considered. Herein, the material properties and sensor device characteristics will now be detailed, followed by a description of the H_2O and NH_3 sensing results for each of the sensor types studied.

3.1. Material & Device Characterisation

Scanning electron microscopy (SEM) showed the different grain sizes and morphologies for the control sample and VO_2(B)–CNT composites (Fig. 2b-d). The VO_2(B) control sample contained both large nanoparticles with features of the order of 1500 nm ± 812 nm, as well as distinctively smaller nanoparticles of 428 nm ± 147 nm dimension. The side lengths of the VO_2(B)-CNT samples were typically of the order of 150 nm ± 48 nm. The distribution of analysed particle sizes, along with descriptive statistics, are presented in the supporting information. Transmission electron microscopy (TEM) confirmed the presence of CNTs in the composite samples (Fig. 2e-f) and that the diameters of the nanotubes were within the range expected (see supporting information).

The bulk of the VO_2(B) nanoparticles produced *via* the CHFS method were monoclinic B-phase (similar to the ICSD database reference pattern 73856 and the study by Popuri *et al*.[55]), as confirmed by powder X-Ray diffraction (Fig. 3). XPS analysis showed that vanadium was present in both the V^{4+} and V^{5+} oxidation states on the surface of the VO_2(B) nanoparticles[56]. This could be attributable to surface VO_2 and V_2O_5, as well as hydroxyl groups and adsorbates that are not removed by preliminary treatments. Previous studies have reported the formation of surface V_2O_5 in VO_2(B) samples[56]. The surface V^{4+}/V^{5+} ratio was 1.1 ± 0.05, 1.2 ± 0.05 and 1.3 ± 0.05 for the VO_2(B) control, VO_2(B)-SWCNT and VO_2(B)-MWCNT samples respectively (Fig. 4a). After N-doping (*via* ammonolysis treatment) nitrogen-hydrogen environments were present on the surfaces of all of the samples, whilst an additional nitrogen-carbon environment was present for the carbon nanotube containing composite samples (Fig. 4c). Additionally, the relative amount of surface V^{5+} increased after the N-doping treatment, with the V^{4+}/V^{5+} ratios now at 0.33 ± 0.05 for the VO_2(B) sample, 0.75 ± 0.05 and 0.58 ± 0.05 for the VO_2(B)-SWCNT and VO_2(B)-MWCNT samples respectively (Fig. 4b).

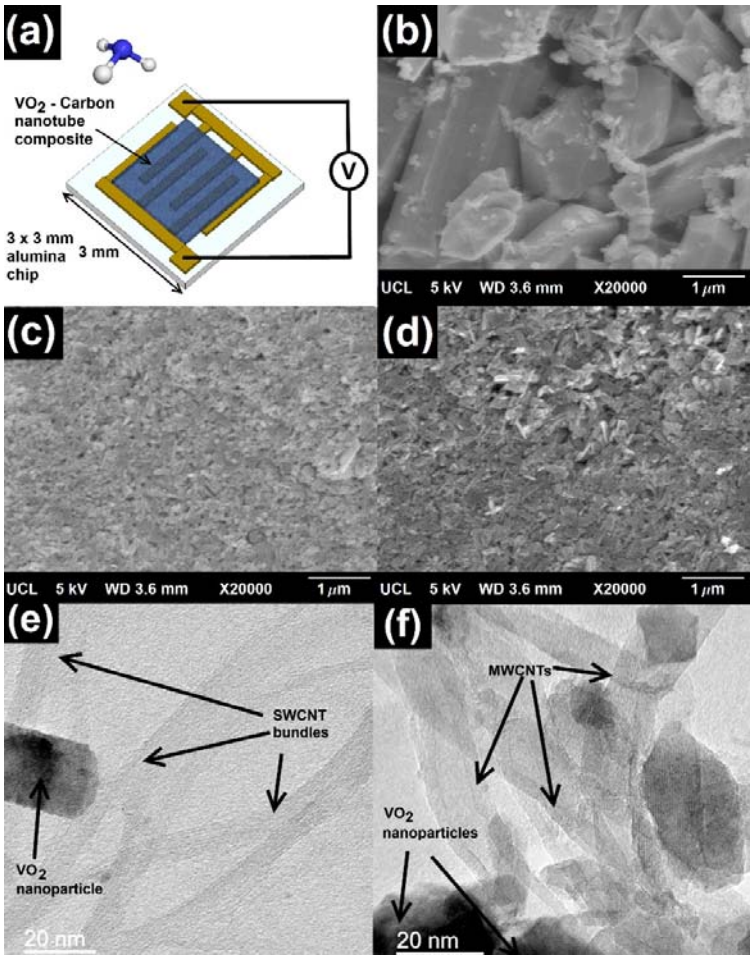

Figure. 2. (a) A schematic of the sensor substrate, the sensing layer and a resistance measurement made across interdigitated gold electrodes with an NH_3 molecule in the surrounding environment (b) an SEM micrograph of a VO_2 sensor surface x20000 magnification (c) SEM micrograph of VO_2 - SWCNT sensor surface x20000 magnification (d) SEM micrograph of VO_2 - MWCNT sensor surface x20000 magnification (e) TEM showing SWCNTs and (f) MWCNTs present in the respective VO_2 composites.

BET analysis showed the surface areas of the VO_2(B) control, VO_2(B)-SWCNT and VO_2(B)-MWCNT were ca. 26, 8 and 18 $m^2\ g^{-1}$, respectively.

In the blank un-doped VO_2(B) sample, the average resistance was variable between repeat devices (2.1 MΩ ± 83 %). The resistance of the un-doped VO_2(B)-MWCNT sensors also displayed a large variation (10.9 MΩ ± 75 %), whilst the resistance of the VO_2(B)-SWCNT sensors (81 kΩ ± 20 %) was two orders of magnitude lower than the VO_2(B) control, with reduced device to device variation in resistance. Post N-doping, the resistance of the VO_2(B) control sensors remained unaffected (3.34 MΩ ± 30 %), whereas the resistance of the VO_2(B) -SWCNT and VO_2(B) -MWCNT based devices increased by at least 3 orders of magnitude (1.62 GΩ ± 14 %, 4.08 GΩ ± 24 % respectively). The variation in resistance between repeat devices, was significantly reduced after N-doping, as shown by the reduced error in average sensor baseline resistance values. The room temperature *I-V* curves for all of the sensors studied are available in the supporting information (Fig. S1).

The hot-probe method as discussed by Golan *et al*[54] was used to elucidate the majority charge carrier type in the VO_2(B) control and nanotube modified composite. As displayed in Fig. S8 in the supporting information, a positive increase in the potential across the surface was observed when the hot-probe was applied. This corresponds to electrons as the majority charge carriers and is in line with previous studies in which VO_2(B) was found to be *n*-type.

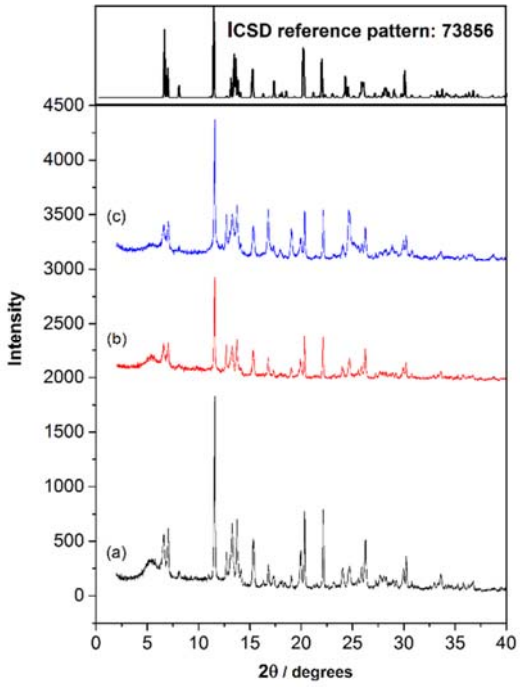

Figure. 3. X-ray diffraction pattern for (a) VO_2 (b) VO_2 – SWCNT composite and (c) VO_2 – MWCNT composite showing the VO_2 bulk material is monoclinic in the B-phase (by comparison to the ICSD database reference pattern: 73856 and to the study by Popuri *et al*.[55]).

3.2. p-type Sensing Responses

Conductivity type plays an important role in sensor responses for metal-oxide nanomaterial based sensors[57]. Both VO_2(B) and V_2O_5 are usually considered to be *n*-type semiconductors at room temperature[58–60]. This was confirmed for the CHFS produced VO_2 materials under investigation in the current study using the hot-probe method (Fig. S8 in the supporting information). However, both *p*-type and *n*-type sensing behaviour for VO_x based sensors has been reported previously, depending on the temperature of operation and the surface species present in the sample[12,14,24,25].

The VO_2(B) control sensors in the current study demonstrated small *p*-type decreases in resistance (ΔR = -1.4 %) when more O_2 was delivered to the sensor surface (achieved by increasing the flow of synthetic air containing O_2 from 25 to 100 % of maximum flow rate (see Fig. S2 in the supporting information). Furthermore, the responses to H_2O (Fig. 5) and NH_3 (Fig. 7) correspond to *p*-type increases in resistance upon chemisorption of a reducing species for all of the VO_2 based sensors. This intriguing *p*-type gas sensing behaviour from *n*-type VO_2(B) has previously been attributed to the formation of an inversion layer on the surface of the metal oxide[61].

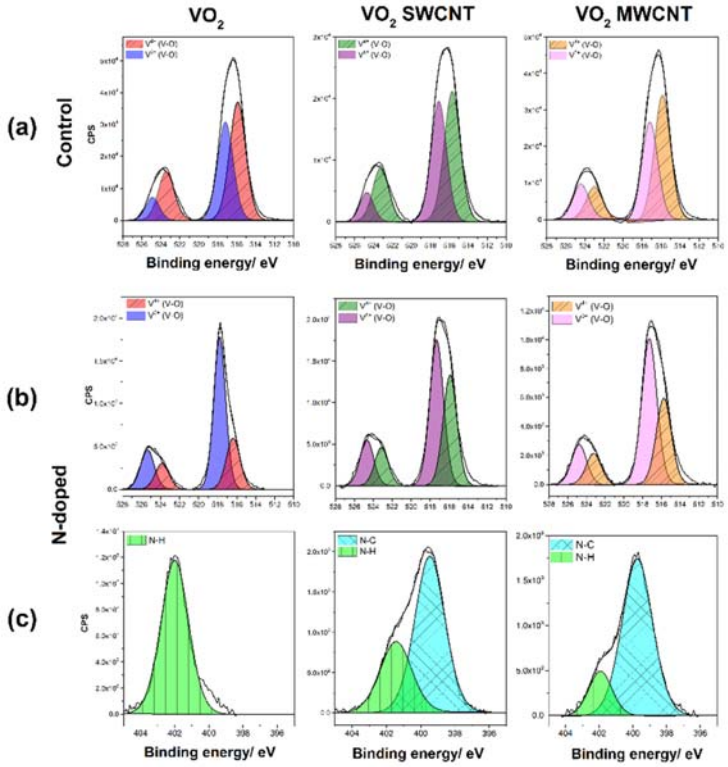

Figure. 4. X-Ray photoelectron spectroscopy results showing (a) vanadium (2p) scan for VO_2 control and VO_2-CNT samples (b) a vanadium (2p) scan for the respective N-doped samples and (c) a carbon (1s) scan for the N-doped samples. Data was calibrated against the C1s signal (285.0 eV).

3.3. Sensitivity to Water Vapour

The VO_2(B)-SWCNT and VO_2(B)-MWCNT composite sensors were highly sensitive to water vapour (S = 2.7 and S = 3.6 respectively, when increasing RH to 50 %, see Fig. 5). As the relative humidity (RH) of the sensing chamber was increased from 0 to 90 %, a large non-linear increase in the resistance of the sensors was observed (Fig. 6a).

The VO_2(B) control samples showed much less sensitivity to water vapour (S = 0.25 at RH = 50 %), indicating that the incorporation of carbon nanotubes drastically increased the sensitivity to water vapour. The resistance increase observed at lower RH for the VO_2(B) control sensors switched to a resistance decrease at humidities >50 % (Fig. 5a), which may be due to an increased response contribution from the bulk *n*-type material in competition with the hypothesised *p*-type surface inversion layer.

BET measurements showed that the VO_2(B) control had a higher surface area, which may explain the switch in sensing behaviour from increasing to deceasing resistance for the VO_2 control sensors at higher humidities. A higher water adsorption capacity would facilitate more displacement of surface adsorbed oxygen, removing an inversion layer at higher humidities and resulting in the switch from *p*-type to *n*-type responses for VO_2(B) control sensors.

P-type responses from *n*-type metal oxide semiconducting based sensors operating at both room[62,63] and elevated temperatures[64,65], have been reported previously. The switching from *n*-type to *p*-type responses is often attributed to the interaction of the target gas with surface adsorbed oxygen species or water[64]. Qin *et al.* and Tutov *et al.* proposed that the *p*-type responses observed for *n*-type V_2O_5 hierarchical networks and VO_2(B) thin films, respectively, were due to the formation of an inversion layer[25,61]. In the study by Dey *et al.*, sensors fabricated from VO_2(B) displayed a decrease in resistance when exposed to increasing levels of humidity and the material was treated as *n*-type. However, Yin *et al.* observed a resistance increase using flower-like VO_2(B) nanostructures, as did Tutov *et al.* with VO_2(B) films, which is therefore in agreement with the current study. These contrasting results suggest that the sensing response type of VO_2(B) at room temperature, is highly dependent on synthesis procedure and the resultant surface species.

The VO_2-CNT composites always displayed a *p*-type increase in resistance over the whole range of relative humidities studied, in contrast to the VO_2(B) control samples. Furthermore, the responses observed for the composite sensors were an order of magnitude larger than those of the VO_2 control sample (Fig. 6a). The sensitivity of carbon nanotubes to water vapour is well reported[66–68]. As the nanotubes contribute significantly towards conduction in the composites, any interactions inducing changes in conductance of the tubes, will have a large overall effect on the resistance of the sensor, which may have been the cause of the larger responses to water. Secondly, the addition of the nanotubes to the surface of the sensing layer, which normally demonstrate *p*-type sensing behavior, may have aided the formation of the inversion layer proposed by Qin *et al.*, increasing *p*-type responses to water vapour.

Response recovery was good for the VO_2(B)-CNT composites after exposure to water (30 s), with response characteristics comparing well to those observed for other room temperature humidity sensors (a comparison with results from the literature is presented in Table. 1). Some drift in baseline resistance was observed for the VO_2(B)-CNT composites, but a more profound drift was apparent for the VO_2(B) control sensors.

Ammonolysis treatment was used to N-dope the VO_2(B), VO_2(B)-SWCNTs and VO_2(B)-MWCNTs samples. The average resistances of the devices fabricated using the N-doped VO_2(B)-CNT composite were three orders of magnitude larger (Fig. S1, supporting information) than the un-doped composite sensors. Interestingly, N-doping did not have any effect on the resistance of the VO_2 control sensors (when variations in the resistances of identical devices were accounted for).

The responses to water for the VO_2-MWCNT and VO_2-SWCNT sensors decreased after N-doping (Fig. 5a-c), especially at high relative humidities (by a factor of 10 and 2 respectively at 50 % RH, by factor 100 and 10 at 70 % RH, see Fig. 6). The N-doping increased the water sensitivity of the VO_2 control sensors to levels comparable with the N-doped VO_2-CNTs sensors (Fig. 6b). Therefore, N-doping appears to contrastingly influence the resistance-humidity responses of the VO_2 control *vs* VO_2-CNT samples. This may be due to a reduced *p*-type contribution from the nanotubes for the VO_2-CNT sensor responses to water vapour after N-doping.

Both VO_2-CNT sensors now displayed a linear increase in resistance as the RH of the sensing chamber was increased (Fig. 6b). The VO_2 control (no carbon) also displayed a linear increase in resistance over the full range of humidities investigated after N-doping, with no reversed response above 50 % RH, as seen in the un-doped VO_2 control sample. Therefore, N-doping treatment appeared to nullify any effect the nanotubes had on sensor responses to water vapour, with all three N-doped sensor types showing a similar linear increase in resistance as a function of increasing humidity levels. Furthermore, it prevented the response switching behaviour seen at higher humidities in the VO_2(B) control sensors. This could be due to a change in the molecular species present or the amount of V_2O_5 on the surface of the VO_2(B) nanoparticles, as evidenced from XPS by the large change in the ratio of V^{4+} / V^{5+} oxidation states.

Table. 1. Comparison of various resistive sensor responses (defined as $S = |(R - R_0) / R_0)|$), response and recovery times to H_2O vapour and NH_3 gas at room temperature for other metal oxide, CNT or composite sensing systems. *indicates the VO_2 based materials used in the current study.

Metal oxide or CNT based nanomaterial	Resistive Response to H_2O	Resistive Response to NH_3	Response Time (H_2O, NH_3)	Recovery Time (H_2O, NH_3)
VO_2(B)*	0.5 (50 % RH)	0.1 (45 ppm)	5 s, 310 s	30 s, 40 min
VO_2-SWCNT*	2.7 (50 % RH)	0.04 (45 ppm)	10 s, 295 s	60 s, 30 min
VO_2-MWCNT*	7.1 (50 % RH)	0.04 (45 ppm)	7 s, 290 s	60 s, 30 min
VO_2(B) nanoflowers[14]	2.0 (50 % RH)	-	40 s, -	50 s, -
$W_{18}O_{49}$ NW[62]	-	0.06 (45 ppm)	-, -	-, -
In_2O_3 NW[69]	-	2000 (25 ppm)	-, -	-, -

Ag NC–MWCNTs[70]	-	0.08 (1% flow)	-, -	-, -
SnO_2-rGO[71]	-	0.3 (200 ppm)	-, 8 s	-, 12 s
WO_3 NW[72]	0.02 (50 % RH)	-	-, -	-, -
WO_3 thin film[73]	0.22 (50 % RH)	-	-, -	-, -
PI/MWNT[48]	0.04 (50 % RH)	-	5 s, -	5 s, -
NiO-SnO_2[74]	0.5 (50 % RH)	-	30 s, -	45 s, -

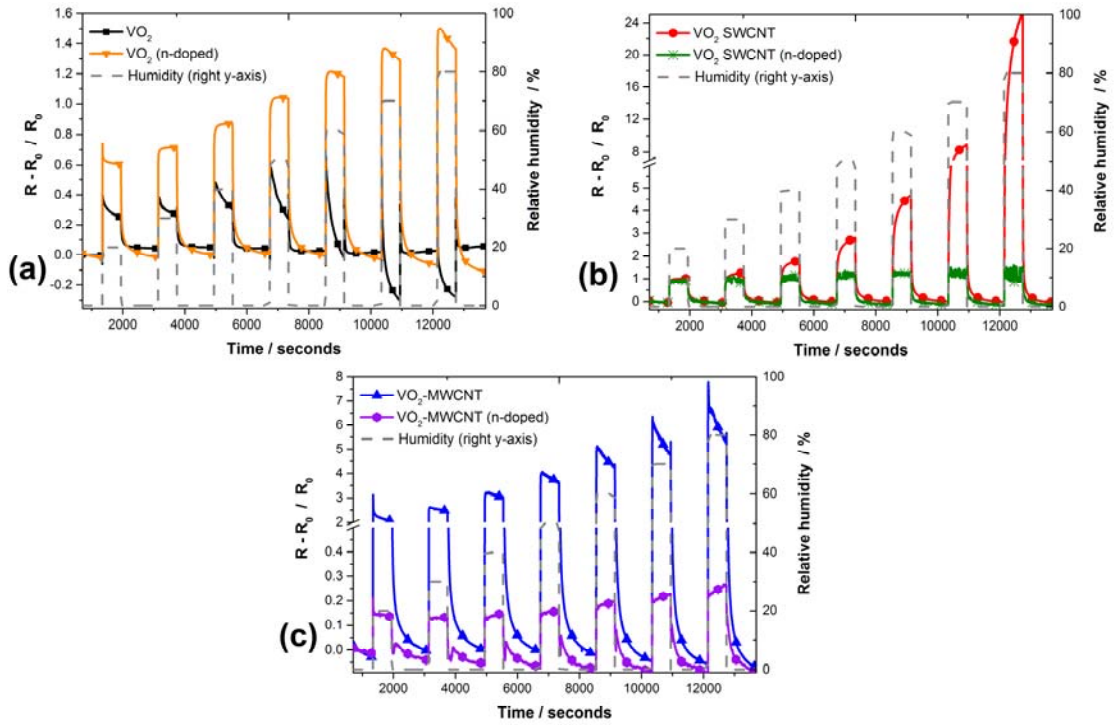

Figure. 5. Real time sensor response curves showing examples of the resistance changes observed (plotted as response magnitude $S = (R - R_0) / R_0$, left y-axis) when un-doped or N-doped (a) VO_2 control (no carbon) sensors (b) VO_2-SWCNT sensors and (c) VO_2-MWCNT sensors are exposed to increasing levels of relative humidity in the sensing chamber. The relative humidity within the sensing chamber is indicated by the dashed grey line and the right y-axis. Left y-axis scale breaks in plot (b) and (c) are used to enable clear comparison of response magnitudes between un-doped and N-doped responses.

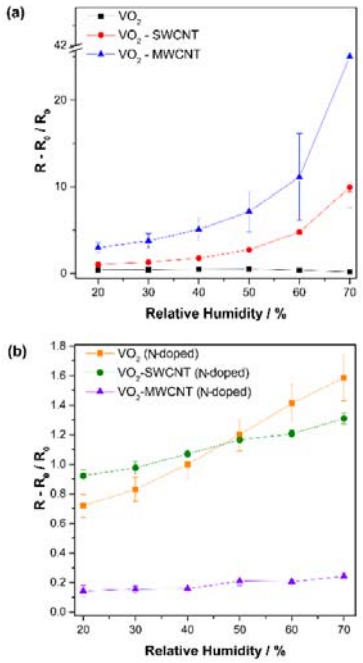

Figure. 6. (a) The sensor response magnitudes to water vapour for the (a) VO_2 control (no carbon), VO_2-MWCNT and VO_2-SWCNT sensors and for (b) the N-doped version of each sensor type. The relative humidity of the sensing chamber was increased from 20 to 70 %. The responses were averaged over the three cycles and the error bars represent the standard error on the mean response at each RH %. A y-axis scale break is used in plot (a) to include the full error bar range for the VO_2-MWCNT sensor.

3.4. Sensitivity to Ammonia Gas

Generally, the sensitivity of metal oxides to electron rich gases such as ammonia (NH_3) at room temperature, can be attributed to the formation of an O_2^- depletion layer on the surface[12]. In such gas sensors, NH_3 reacts with the surface adsorbed oxygen, releasing electrons and inducing an electrical response to a changing gaseous environment. For *p*-type materials, electron donation reduces the number of holes (the majority charge carriers), resulting in a *p*-type increase in device resistance[12]. However, as discussed in the previous section, VO_2 is normally considered to be an *n*-type semiconductor at room temperature[58–60]. Once again, the formation of a surface inversion layer would explain the anomalous *p*-type responses of the VO_2 based sensors toward NH_3.

From Fig. 7a, it is clear that the VO_2 control sensors demonstrated the largest responses amongst those tested and that some signal drift occurred, indicating chemisorption of NH_3. This hypothesis was supported by ATR-FTIR measurements (Fig. S9 in the supporting information), which suggests surface formation of NH_4^+ after exposing the samples to 50 ppm of NH_3 for 30 min. The appearance of the band at 1409 cm^{-1} (the N-H in-plane bending vibration mode)[75] has previously been attributed to the formation of NH_4^+ ions[76], which would cause drift in the baseline resistance of the sensing layer. There was little difference between the response magnitudes observed for the VO_2-CNT sensors, even though the sensors containing SWCNTs were much less resistive (by a factor of at least 10) than those containing MWCNTs (Fig. 7b). This suggests that these much smaller responses to NH_3 (when compared to those induced by varying relative humidity) are unaffected by the type or conductivity of the tubes present in the VO_2 sensing layer, and thus, that responses to NH_3 are due to reactions between the vanadium oxides surface species and ammonia gas. With this in mind, it is thought that the larger responses observed for the VO_2 control sensors are due to the higher surface area of the VO_2 control sample (as confirmed by BET measurements), resulting in more surface oxygen-ammonia chemisorption reactions.

To further investigate the apparent *p*-type behavior, a VO_2(B) control (no carbon) sensor was exposed to 1 ppm NO_2 gas. A resistance decrease was observed, consistent with a *p*-type response to NO_2 (oxidising) gas. This confirms the *p*-type nature of the sensing responses for the VO_2(B) control (no carbon) sensors used in this study.

Fig. S4 in the supporting information shows that responses of the VO_2(B) control (no carbon) sensors are slightly reduced after N-doping. XPS analysis indicates a higher proportion of surface V^{5+} after N-doping treatment. Different relative amounts of oxygenated surface species may contribute toward a reduced NH_3 response for the N-doped VO_2 sensors. A decreased

signal to noise ratio for the N-doped VO_2(B)-CNT samples was observed for responses to NH_3, presumably due to the large increase in bassline resistance of the samples.

3.5. NH_3 and H_2O Sensing Applications

Detection of gaseous NH_3 within 1 min is typically required, at concentrations in the range of 20 ppb to 200 ppm for general environmental monitoring[77], 1 ppm to 20 ppm for agricultural monitoring[78] and 20 ppm to 2000 ppm for safety alerts in industrial processes[79]. For breath analysis[80] the relevant range is 20 ppb to 2 ppm. With this in mind, the VO_2 based sensors would be suitable for industrial safety monitoring. Increasing the surface area available for NH_3–surface interactions *via* optimization of the CHFS process, may decrease the limit of detection to the ppb range for medical diagnosis applications. One important issue that must be addressed is the drift in sensor response (as shown in Fig. 7a) after exposure to NH_3, which may be reduced by techniques such as cycled Ohmic heating. The response magnitudes and characteristics compare well with results from similar devices presented in the literature, as displayed in Table. 1.

As shown in Fig. S13, the sensors studied demonstrate cross-sensitivity 1 ppm concentrations of NO_2 gas. The decrease in resistance of the sensors upon exposure to an oxidising analyte is in line with *p*-type sensing behaviour. Cross-sensitivity to oxidising gases is a common problem for metal oxide based sensors in passive sampling applications. This could be limited by adding a filter layer to the sensor housing, or incorporating the sensors into a discriminatory array.

A linear resistive response to increases in relative humidity, such as those demonstrated by the N-doped VO_2 sensors, is desirable for humidity sensors as it simplifies integrated circuit design and sensor data processing[47]. Furthermore, the fast responses (<10 s) to water vapour, low cost and low power consumption of the VO_2 based devices that operate at room temperature, makes them potential candidates for a variety of applications as detailed by Blank *et al*[47]. However, further improvements are needed; overcoming the drift in sensor baseline signal would be a priority to move toward such practical applications, as well as incorporating commercially scalable screen printing methods into the sensor fabrication process.

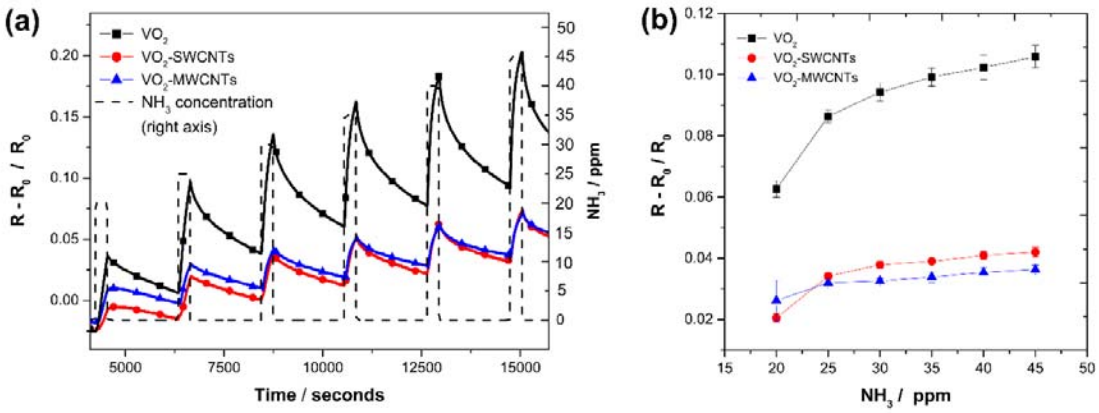

Figure. 7. (a) Real time sensing response curves showing examples of the resistance changes observed (plotted as response magnitude $S = (R - R_0) / R_0$) when un-doped VO_2 control sensors, VO_2-SWCNT sensors and VO_2-MWCNT sensors are exposed to increasing concentrations of NH_3. The sensor response magnitudes averaged over three testing cycles are shown in (b) for NH_3 concentrations (in dry synthetic air) in the range 20 to 45 ppm. The error bars represent the standard error on the mean response magnitudes to NH_3.

4. Conclusion

Continuous hydrothermal flow synthesis was successfully used to make VO_2(B) and VO_2(B)-CNT nanocomposite materials that were investigated for gas sensing applications (at room temperature). The surface compositions and microstructures of the respective nanomaterials were found to greatly influence the sensor responses to water vapour and ammonia gas. XPS analysis indicated that the nanoparticles comprised of a heterogeneous vanadium oxide surface layer with a variety of surface species, whilst XRD studies established that the nanoparticle bulk consisted of VO_2(B). The resistances of the VO_2(B) based devices, were reduced upon incorporation of the CNTs (in some cases by two orders of magnitude), indicating that the CNTs significantly contributed to conductance in the composite material. Although the VO_2(B) synthesis in this study, was confirmed to be an *n*-type semiconductor using the hot-probe method[54], *p*-type responses to water vapour

were observed for the VO_2 based sensors. Similar studies have attributed such behavior to the formation of a surface inversion layer, which was suggested as a possible explanation for the *p*-type sensing results in the current work.

The addition of carbon nanotubes to the VO_2 sensing layer, was found to greatly increase sensitivity to water vapour. This increase was attributed to the dependency of the nanocomposite materials' overall resistance on the electronic properties of the carbon nanotubes, which are known to be sensitive to the relative humidity of the sensing environment. Both VO_2(B) and VO_2(B)-CNT sensors demonstrated *p*-type responses to NH_3 in the 10 to 50 ppm range. The larger responses observed toward NH_3 for the VO_2(B) control (no carbon) sensors were attributed to the higher surface area of the control material, as confirmed by BET analysis. N-doping the composite samples, reduced the impact that the CNTs had on water sensitivity, with N-doped composite sensors showing response characteristics that were comparable to the N-doped VO_2(B) control sensors. Furthermore, a relative change in the amount of surface V^{5+} was observed after N-doping treatment, which contributed towards a reduced NH_3 response for the VO_2(B) control (no carbon) sensors. These results suggested that CHFS produced VO_2(B)-CNT composite nanomaterials were highly sensitive to water vapour and showed promise for use in humidity sensing applications. Conversely, the larger surface areas of the CHFS produced VO_2(B) control samples in this study, made them the superior choice for use in room temperature NH_3 sensors.

Acknowledgements

The authors thank Dr. Steve Firth for instrumentation assistance. This work was carried out under EPSRC Grant EP/G037264/1 as part of UCL's Security Science Doctoral Training Centre.

Supporting Information

Additional XPS, TEM, SEM and ATR-FTIR data is available in the supporting information. I-V characterisation, hot-probe method data and complimentary gas sensing results are also included.

References

1. Fam, D. W. H., Palaniappan, A., Tok, A. I. Y., Liedberg, B. & Moochhala, S. M. A review on technological aspects influencing commercialization of carbon nanotube sensors. *Sens. Actuators B Chem.* **157,** 1–7 (2011).
2. Naik, A. J. T. *et al.* Environmental sensing semiconducting nanoceramics made using a continuous hydrothermal synthesis pilot plant. *Sens. Actuators B Chem.* **217,** 136–145 (2015).
3. Llobet, E. Gas sensors using carbon nanomaterials: A review. *Sens. Actuators B Chem.* **179,** 32–45 (2013).
4. Jiménez-Cadena, G., Riu, J. & Rius, F. X. Gas sensors based on nanostructured materials. *Analyst* **132,** 1083–1099 (2007).
5. Ramgir, N. S., Yang, Y. & Zacharias, M. Nanowire-Based Sensors. *Small* **6,** 1705–1722 (2010).
6. Zhang, J., Liu, X., Neri, G. & Pinna, N. Nanostructured Materials for Room-Temperature Gas Sensors. *Adv. Mater.* **28,** 795–831 (2016).
7. Ellis, J. E. & Star, A. Carbon Nanotube-based Gas Sensors toward Breath Analysis. *ChemPlusChem* 1248–1265 (2016). doi:10.1002/cplu.201600478

8. Su, S., Wu, W., Gao, J., Lu, J. & Fan, C. Nanomaterials-based sensors for applications in environmental monitoring. *J. Mater. Chem.* **22,** 18101–18110 (2012).
9. Khot, L. R., Sankaran, S., Maja, J. M., Ehsani, R. & Schuster, E. W. Applications of nanomaterials in agricultural production and crop protection: A review. *Crop Prot.* **35,** 64–70 (2012).
10. Korotcenkov, G. Metal oxides for solid-state gas sensors: What determines our choice? *Mater. Sci. Eng. B* **139,** 1–23 (2007).
11. Powell, M. J. *et al.* Direct and continuous synthesis of VO2 nanoparticles. *Nanoscale* **7,** 18686–18693 (2015).
12. Dey, K. K. *et al.* VO2 nanorods for efficient performance in thermal fluids and sensors. *Nanoscale* **7,** 6159–6172 (2015).
13. Strelcov, E., Lilach, Y. & Kolmakov, A. Gas Sensor Based on Metal−Insulator Transition in VO_2 Nanowire Thermistor. *Nano Lett.* **9,** 2322–2326 (2009).
14. Yin, H. *et al.* Humidity Sensing Properties of Flower-Like VO2(B) and VO2(M) Nanostructures. *Electroanalysis* **23,** 1752–1758 (2011).
15. Simo, A. *et al.* VO2 nanostructures based chemiresistors for low power energy consumption hydrogen sensing. *Int. J. Hydrog. Energy* **39,** 8147–8157 (2014).
16. Raible, I., Burghard, M., Schlecht, U., Yasuda, A. & Vossmeyer, T. V2O5 nanofibres: novel gas sensors with extremely high sensitivity and selectivity to amines. *Sens. Actuators B Chem.* **106,** 730–735 (2005).
17. Liu, J., Wang, X., Peng, Q. & Li, Y. Vanadium Pentoxide Nanobelts: Highly Selective and Stable Ethanol Sensor Materials. *Adv. Mater.* **17,** 764–767 (2005).
18. Zhang, Z., Kaneti, Y. V., Jiang, X. & Yu, A. Hydrothermal synthesis of sodium vanadium oxide nanorods for gas sensing application. *Sens. Actuators B Chem.* **202,** 803–809 (2014).
19. Vieira, N. C. S., Avansi Jr., W., Figueiredo, A., Mastelaro, V. R. & Zucolotto, V. Potentiometric detection of chemical species by spin-assisted assembly of vanadium pentoxide nanorods. *Sens. Actuators B Chem.* **229,** 461–465 (2016).
20. Dhayal Raj, A. *et al.* Self assembled V2O5 nanorods for gas sensors. *Curr. Appl. Phys.* **10,** 531–537 (2010).
21. Shimizu, K. *et al.* Doped-vanadium oxides as sensing materials for high temperature operative selective ammonia gas sensors. *Sens. Actuators B Chem.* **141,** 410–416 (2009).

22. Modafferi, V. *et al.* Highly sensitive ammonia resistive sensor based on electrospun V2O5 fibers. *Sens. Actuators B Chem.* **163,** 61–68 (2012).
23. Huotari, J., Bjorklund, R., Lappalainen, J. & Lloyd Spetz, A. Pulsed Laser Deposited Nanostructured Vanadium Oxide Thin Films Characterized as Ammonia Sensors. *Sens. Actuators B Chem.* **217,** 22–29 (2015).
24. Yu, M. *et al.* Gas sensing properties of p-type semiconducting vanadium oxide nanotubes. *Appl. Surf. Sci.* **258,** 9554–9558 (2012).
25. Qin, Y., Fan, G., Liu, K. & Hu, M. Vanadium pentoxide hierarchical structure networks for high performance ethanol gas sensor with dual working temperature characteristic. *Sens. Actuators B Chem.* **190,** 141–148 (2014).
26. Prasad, A. K. *et al.* Novel single phase vanadium dioxide nanostructured films for methane sensing near room temperature. *Sens. Actuators B Chem.* **191,** 252–256 (2014).
27. Karimov, K. S. *et al.* Resistive humidity sensor based on vanadium complex films. *J. Semicond.* **35,** 094001 (2014).
28. Li, W., Ma, Y., Ji, S., Sun, G. & Jin, P. Synthesis and humidity sensing properties of the VO2(B)@ZnO heterostructured nanorods. *Ceram. Int.* **42,** 9234–9240 (2016).
29. Snow, E. S., Perkins, F. K. & Robinson, J. A. Chemical vapor detection using single-walled carbon nanotubes. *Chem. Soc. Rev.* **35,** 790 (2006).
30. Kauffman, D. R. & Star, A. Carbon Nanotube Gas and Vapor Sensors. *Angew. Chem. Int. Ed.* **47,** 6550–6570 (2008).
31. Goldoni, A., Petaccia, L., Lizzit, S. & Larciprete, R. Sensing gases with carbon nanotubes: a review of the actual situation. *J. Phys. Condens. Matter* **22,** 013001 (2010).
32. Sun, Y.-P., Fu, K., Lin, Y. & Huang, W. Functionalized Carbon Nanotubes: Properties and Applications. *Acc. Chem. Res.* **35,** 1096–1104 (2002).
33. Schnorr, J. M., van der Zwaag, D., Walish, J. J., Weizmann, Y. & Swager, T. M. Sensory Arrays of Covalently Functionalized Single-Walled Carbon Nanotubes for Explosive Detection. *Adv. Funct. Mater.* **23,** 5285–5291 (2013).
34. Bekyarova, E. *et al.* Chemically Functionalized Single-Walled Carbon Nanotubes as Ammonia Sensors. *J. Phys. Chem. B* **108,** 19717–19720 (2004).
35. Qi, P. *et al.* Toward large arrays of multiplex functionalized carbon nanotube sensors for highly sensitive and selective molecular detection. *Nano Lett.* **3,** 347–351 (2003).

36. Frazier, K. M. & Swager, T. M. Robust Cyclohexanone Selective Chemiresistors Based on Single-Walled Carbon Nanotubes. *Anal. Chem.* **85,** 7154–7158 (2013).
37. Evans, G. P. *et al.* Controlling the Cross-Sensitivity of Carbon Nanotube-Based Gas Sensors to Water Using Zeolites. *ACS Appl. Mater. Interfaces* **8,** 28096−28104 (2016).
38. Evans, G. P., Buckley, D. J., Skipper, N. T. & Parkin, I. P. Single-walled carbon nanotube composite inks for printed gas sensors: enhanced detection of NO 2, NH 3, EtOH and acetone. *RSC Adv.* **4,** 51395–51403 (2014).
39. Mendoza, F. *et al.* Room temperature gas sensor based on tin dioxide-carbon nanotubes composite films. *Sens. Actuators B Chem.* **190,** 227–233 (2014).
40. Chen, H.-W., Wu, R.-J., Chan, K.-H., Sun, Y.-L. & Su, P.-G. The application of CNT/Nafion composite material to low humidity sensing measurement. *Sens. Actuators B Chem.* **104,** 80–84 (2005).
41. Daniel, S. *et al.* A review of DNA functionalized/grafted carbon nanotubes and their characterization. *Sens. Actuators B Chem.* **122,** 672–682 (2007).
42. Willinger, M.-G. *et al.* Vanadium Oxide Sensing Layer Grown on Carbon Nanotubes by a New Atomic Layer Deposition Process. *Nano Lett.* **8,** 4201–4204 (2008).
43. Faia, P. M., Libardi, J. & Louro, C. S. Effect of V2O5 doping on p- to n-conduction type transition of TiO2:WO3 composite humidity sensors. *Sens. Actuators B Chem.* **222,** 952–964 (2016).
44. Shi, L. *et al.* Highly Sensitive ZnO Nanorod- and Nanoprism-Based NO2 Gas Sensors: Size and Shape Control Using a Continuous Hydrothermal Pilot Plant. *Langmuir* **29,** 10603–10609 (2013).
45. Elouali, S. *et al.* Gas Sensing with Nano-Indium Oxides (In2O3) Prepared via Continuous Hydrothermal Flow Synthesis. *Langmuir* **28,** 1879–1885 (2012).
46. Gruar, R. I., Tighe, C. J. & Darr, J. A. Scaling-up a Confined Jet Reactor for the Continuous Hydrothermal Manufacture of Nanomaterials. *Ind. Eng. Chem. Res.* **52,** 5270–5281 (2013).
47. Blank, T. A., Eksperiandova, L. P. & Belikov, K. N. Recent trends of ceramic humidity sensors development: A review. *Sens. Actuators B Chem.* **228,** 416–442 (2016).
48. Tang, Q. Y., Chan, Y. C. & Zhang, K. Fast response resistive humidity sensitivity of polyimide/multiwall carbon nanotube composite films. *Sens. Actuators B Chem.* **152,** 99–106 (2011).

49. Howard, D. P. *et al.* Conducting Al and Ga-doped zinc oxides; rapid optimisation and scale-up. *J. Mater. Chem. A* **4,** 12774–12780 (2016).
50. Breeson, A. C., Sankar, G., Goh, G. K. L. & Palgrave, R. G. Rutile to anatase phase transition induced by N doping in highly oriented TiO2 films. *Phys. Chem. Chem. Phys.* **18,** 24722–24728 (2016).
51. Mumyakmaz, B., Özmen, A., Ebeoğlu, M. A., Taşaltın, C. & Gürol, İ. A study on the development of a compensation method for humidity effect in QCM sensor responses. *Sens. Actuators B Chem.* **147,** 277–282 (2010).
52. Fratoddi, I., Bearzotti, A., Venditti, I., Cametti, C. & Russo, M. V. Role of nanostructured polymers on the improvement of electrical response-based relative humidity sensors. *Sens. Actuators B Chem.* **225,** 96–108 (2016).
53. Takahashi, C. & Kitano, H. Calibration method of flow meters for a divided flow humidity generator. *Sens. Actuators B Chem.* **36,** 522–527 (1996).
54. Golan, G., Axelevitch, A., Gorenstein, B. & Manevych, V. Hot-Probe method for evaluation of impurities concentration in semiconductors. *Microelectron. J.* **37,** 910–915 (2006).
55. Popuri, S. R. *et al.* Rapid Hydrothermal Synthesis of VO2 (B) and Its Conversion to Thermochromic VO2 (M1). *Inorg. Chem.* **52,** 4780–4785 (2013).
56. Silversmit, G., Depla, D., Poelman, H., Marin, G. B. & De Gryse, R. Determination of the V2p XPS binding energies for different vanadium oxidation states (V5+ to V0+). *J. Electron Spectrosc. Relat. Phenom.* **135,** 167–175 (2004).
57. Wang, C., Yin, L., Zhang, L., Xiang, D. & Gao, R. Metal Oxide Gas Sensors: Sensitivity and Influencing Factors. *Sensors* **10,** 2088–2106 (2010).
58. Rosevear, W. H. & Paul, W. Hall Effect in VO2 near the Semiconductor-to-Metal Transition. *Phys. Rev. B* **7,** 2109–2111 (1973).
59. Chen, F. H. *et al.* Control of the Metal–Insulator Transition in VO2 Epitaxial Film by Modifying Carrier Density. *ACS Appl. Mater. Interfaces* **7,** 6875–6881 (2015).
60. Barreca, D. Vanadyl Precursors Used to Modify the Properties of Vanadium Oxide Thin Films Obtained by Chemical Vapor Deposition. *J. Electrochem. Soc.* **146,** 551 (1999).
61. Tutov, E. A. & Zlomanov, V. P. Effect of chemisorption of donor and acceptor gases on the semiconductor-metal phase transition in vanadium dioxide films. *Phys. Solid State* **55,** 2351–2354 (2013).

62. Zhao, Y. M. & Zhu, Y. Q. Room temperature ammonia sensing properties of W18O49 nanowires. *Sens. Actuators B Chem.* **137,** 27–31 (2009).

63. Shao, S. *et al.* Regulable switching from p- to n-type behavior of ordered nanoporous Pt-SnO2 thin films with enhanced room temperature toluene sensing performance. *RSC Adv.* **6,** 22878–22888 (2016).

64. Gurlo, A., Sahm, M., Oprea, A., Barsan, N. & Weimar, U. A p- to n-transition on α-Fe2O3-based thick film sensors studied by conductance and work function change measurements. *Sens. Actuators B Chem.* **102,** 291–298 (2004).

65. Korotcenkov, G. *et al.* Acceptor-like behavior of reducing gases on the surface of n-type In2O3. *Appl. Surf. Sci.* **227,** 122–131 (2004).

66. Zahab, A., Spina, L., Poncharal, P. & Marlière, C. Water-vapor effect on the electrical conductivity of a single-walled carbon nanotube mat. *Phys. Rev. B* **62,** 10000–10003 (2000).

67. Cantalini, C. *et al.* Sensitivity to NO2 and cross-sensitivity analysis to NH3, ethanol and humidity of carbon nanotubes thin film prepared by PECVD. *Sens. Actuators B Chem.* **95,** 195–202 (2003).

68. Bell, R. A., Payne, M. C. & Mostofi, A. A. Does water dope carbon nanotubes? *J. Chem. Phys.* **141,** 164703 (2014).

69. Du, N. *et al.* Porous Indium Oxide Nanotubes: Layer-by-Layer Assembly on Carbon-Nanotube Templates and Application for Room-Temperature NH3 Gas Sensors. *Adv. Mater.* **19,** 1641–1645 (2007).

70. Cui, S. *et al.* Fast and Selective Room-Temperature Ammonia Sensors Using Silver Nanocrystal-Functionalized Carbon Nanotubes. *ACS Appl. Mater. Interfaces* **4,** 4898–4904 (2012).

71. Chen, Y., Zhang, W. & Wu, Q. A highly sensitive room-temperature sensing material for NH3: SnO2-nanorods coupled by rGO. *Sens. Actuators B Chem.* **242,** 1216–1226 (2017).

72. Sim, J., Choi, J. & Kim, J. Humidity sensing characteristics of focused ion beam-induced suspended single tungsten nanowire. *Sens. Actuators B Chem.* **194,** 38–44 (2014).

73. Qu, W. & Wlodarski, W. A thin-film sensing element for ozone, humidity and temperature. *Sens. Actuators B Chem.* **64,** 42–48 (2000).

74. Pascariu, P. *et al.* Microstructure, electrical and humidity sensor properties of electrospun NiO–SnO2 nanofibers. *Sens. Actuators B Chem.* **222,** 1024–1031 (2016).

75. Abbood, H. A., Peng, H., Gao, X., Tan, B. & Huang, K. Fabrication of cross-like NH4V4O10 nanobelt array controlled by CMC as soft template and photocatalytic activity of its calcinated product. *Chem. Eng. J.* **209,** 245–254 (2012).

76. Wu, X., Tao, Y., Dong, L. & Hong, J. Synthesis and characterization of self-assembling (NH4)0.5V2O5 nanowires. *J. Mater. Chem.* **14,** 901–904 (2004).

77. Erisman, J. W. *et al.* Instrument development and application in studies and monitoring of ambient ammonia. *Atmos. Environ.* **35,** 1913–1922 (2001).

78. Mount, G. H. *et al.* Measurement of atmospheric ammonia at a dairy using differential optical absorption spectroscopy in the mid-ultraviolet. *Atmos. Environ.* **36,** 1799–1810 (2002).

79. de la Hoz, R. E., Schlueter, D. P. & Rom, W. N. Chronic lung disease secondary to ammonia inhalation injury: A report on three cases. *Am. J. Ind. Med.* **29,** 209–214 (1996).

80. Kearney, D. J., Hubbard, T. & Putnam, D. Breath Ammonia Measurement in Helicobacter pylori Infection. *Dig. Dis. Sci.* **47,** 2523–2530 (2002).

Author Biographies

Gwyn. P. Evans

Gwyn Evans completed his undergraduate Masters degree in Physics from the University of Liverpool in 2012. He is currently pursuing his PhD in the gas sensing group under the supervision of Professor Ivan Parkin in the Department of Chemistry, University College London (UCL). Gwyn's current research interests include nanomaterials for sensing, security technologies and environmental monitoring applications.

Michael. J. Powell

Michael Powell currently works as a Postdoctoral Research Associate at UCL, having achieved a PhD in 2015 under the supervision of Prof Ivan Parkin. His research interests include transparent conducting oxides, photocatalysis, thermochromic and battery materials. Michael's current project is sponsored by the EPSRC and is aimed at scaling aerosol assisted chemical vapour deposition for the sustainable manufacture of materials.

Ian. D. Johnson

Ian Johnson is a PhD Student of the Clean Materials Technology Group at UCL. His research is focused on the scalable synthesis and characterisation of nanomaterials for a range of applications, including energy storage, gas sensing, and transparent conducting oxides. He was inspired to work in these areas by his MSci and BA in Natural Sciences (Chemistry) from the University of Cambridge (UK).

Dougal. P. Howard

Dougal completed his undergraduate Masters degree at University College London in Chemistry and went on to do a PhD in the Clean Materials Technology Group there under the supervision of Professor Jawwad Darr. His research focused on the continuous hydrothermal flow synthesis of various metal oxide nanoparticles for application as transparent conducting oxides, occasionally delving into energy storage and gas sensing, with a particular interest in sustainability and environmental impact awareness.

Dustin Bauer

Dustin Bauer completed a Master of Science in Materials Chemistry at University College London in 2016. He is now studying a PhD at UCL under supervision of Prof. Jawwad A Darr working on Li-ion and Na-ion batteries and hybrid capacitors.

Jawwad. A. Darr

Professor Jawwad A. Darr received his BSc in chemistry from the University of Manchester in 1991. After a Phd and 1 year postdoctoral research in at Imperial College in Synthetic metal-organic chemistry and further postdoctoral research at Nottingham University. He worked as an experimental officer in biomedical materials for two years at Queen Mary University of London (QMUL) at the IRC in Biomedical Materials. From 2001 – 2006, he was holder of an EPSRC Advanced Research fellowship (and lecturer) developing research on "Next Generation Biomedical Materials using Supercritical Fluids". In May 2007, he joined University College London (UCL), Department of Chemistry and was appointed as full pressor in October 2011. He is visiting professor in Biomaterials at COMSATS University, Lahore, and the UCL Knowledge Transfer Champion for the (MAPS faculty). Professor Darr's group is one of the leading exponents of continuous hydrothermal (supercritical water) flow synthesis, CHFS, reactors for the production of nanoceramics and devices. The technology has been developed in numerous publications for high throughput synthesis to scale-up via a CHFS pilot plant process capable of >1kg per hour). Professor Darr has strong interactions with UK industry related to the discovery of new ceramic nanomaterials in energy (solid oxide fuel cells, Na and Li ion batteries, supercapacitors, transparent conducting oxides), materials discovery/catalysis (reduction of CO2, water splitting/oxidation catalysis) and healthcare applications.

Ivan. P. Parkin

Professor Ivan Parkin is dean of mathematical and physical sciences at University College London. He has research interests in new surface coatings for gas sensing. His team have published over 500 research publications.